MOLECULAR IMAGING AND BIOLOGY

Mol Imaging Biol (2019) 21:1200–1209
DOI: 10.1007/s11307-019-01336-3

Published Online: 7 March 2019

WMIS World Molecular Imaging Society

Check for updates

RESEARCH ARTICLE

Texture Analysis on [^{18}F]FDG PET/CT in Non-Small-Cell Lung Cancer: Correlations Between PET Features, CT Features, and Histological Types

Francesco Bianconi,[1] Isabella Palumbo,[2] Mario Luca Fravolini,[1] Rita Chiari,[3] Matteo Minestrini,[4] Luca Brunese,[5] Barbara Palumbo[4]

[1]*Department of Engineering, Università degli Studi di Perugia, Via G. Duranti 93, 06125, Perugia, Italy*
[2]*Section of Radiation Oncology, Department of Surgical and Biomedical Sciences, Università degli Studi di Perugia, Piazza Lucio Severi 1, 06132, Perugia, Italy*
[3]*Department of Medical Oncology, Ospedale Santa Maria della Misericordia, S. Andrea delle Fratte, 06156, Perugia, Italy*
[4]*Section of Nuclear Medicine and Health Physics, Department of Surgical and Biomedical Sciences, Università degli Studi di Perugia, Piazza Lucio Severi 1, 06132, Perugia, Italy*
[5]*Department of Medicine and Health Sciences "Vincenzo Tiberio", Università degli Studi del Molise, Via Francesco De Sanctis 1, 86100, Campobasso, Italy*

Abstract

Purpose: The study aims to investigate the correlations between positron emission tomography (PET) texture features, X-ray computed tomography (CT) texture features, and histological subtypes in non-small-cell lung cancer evaluated with 2-deoxy-2-[^{18}F]fluoro-D-glucose PET/CT.
Procedures: We retrospectively evaluated the baseline PET/CT scans of 81 patients with histologically proven non-small-cell lung cancer. Feature extraction and statistical analysis were carried out on the Matlab platform (MathWorks, Natick, USA).
Results: Intra-CT correlation analysis revealed a strong positive correlation between volume of the lesion (CT_{vol}) and maximum density (CT_{max}), and between kurtosis (CT_{krt}) and maximum density (CT_{max}). A moderate positive correlation was found between volume (CT_{vol}) and average density (CT_{mean}), and between kurtosis (CT_{krt}) and average density (CT_{mean}). Intra-PET analysis identified a strong positive correlation between the radiotracer uptake (SUV_{max}, SUV_{mean}) and its degree of variability/disorder throughout the lesion (SUV_{std}, SUV_{ent}). Conversely, there was a strong negative correlation between the uptake (SUV_{max}, SUV_{mean}) and its degree of uniformity (SUV_{uni}). There was a positive moderate correlation between the metabolic tumor volume (MTV) and radiotracer uptake (SUV_{max}, SUV_{mean}). Inter (PET-CT) correlation analysis identified a very strong positive correlation between the volume of the lesion at CT (CT_{vol}) and the metabolic volume (MTV), a moderate positive correlation between average tissue density (CT_{mean}) and radiotracer uptake (SUV_{max}, SUV_{mean}), and between kurtosis at CT (CT_{krt}) and metabolic tumor volume (MTV). Squamous cell carcinomas had larger volume higher uptake, stronger PET variability and lower uniformity than the other subtypes. By contrast, adenocarcinomas exhibited significantly lower uptake, lower variability and higher uniformity than the other subtypes.

Correspondence to: Francesco Bianconi; *e-mail:* bianco@ieee.org

Conclusions: Significant associations emerged between PET features, CT features, and histological type in NSCLC. Texture analysis on PET/CT shows potential to differentiate between histological types in patients with non-small-cell lung cancer.

Key words: [^{18}F] FDG PET/CT, Radiomics, Non-small-cell lung cancer, Texture analysis

Introduction

Lung cancer is by far the leading cause of cancer-related death in the USA, with an estimated average incidence of 61.5 new cases/year per 100,000 people between 2010 and 2014 [1]. Of these, approximately 85 in 100 are non-small-cell lung cancer (NSCLC) [2]. Unfortunately, the 5-year relative survival of lung cancer is also very low (≈ 18 %), and much lower than the other most common forms of cancer—except pancreatic cancer [1].

Currently, the radiolabelled glucose-analogue 2-deoxy-2-[^{18}F]fluoro-D-glucose ([^{18}F]FDG) is the most common radiopharmaceutical in NSCLC, its uptake in tumor cells depending on the increased number of functional glucose transporters and glycolytic enzymes [3]. Coupled [^{18}F] FDG positron emission tomography/X-ray computed tomography ("PET/CT" in the remainder) is therefore the standard diagnostic tool for lesion detection and characterization, as well as for the clinical staging of patients with NSCLC [4]. In this scenario the quantitative analysis of lung lesions from PET/CT data has received increasing attention in recent years. Radiomics—as it is called—can be defined as the "comprehensive quantification of tumor phenotypes by applying a large number of quantitative image features" [5]. Radiomics has shown potential in a number of tasks such as classifying lung lesions into benign or malignant [6], differentiating between primary and metastatic lesions [7], predicting survival [8–11] and response to treatment [12, 13]. All this shows promise towards personalized therapy in oncology [14]. It is also hoped that radiomics could help unveil hidden patterns and trends that have so far gone unnoticed in the clinical practice: this could ultimately lead to a better understanding of lung cancer as a whole, and pave the way to major breakthroughs in the management of this disorder.

Texture analysis is the process of extracting meaningful and quantitative parameters from two- or three-dimensional images. Such parameters, usually referred to as features, can be processed *via* artificial intelligence methods (*e.g.*, automatic classifiers) and allow for non-invasive quantification of tumor phenotypic characteristics [18]. It is believed, in particular, that the application of texture analysis and artificial intelligence to PET and CT data has the potential not only to enable quantitative, objective, and repeatable measurements but also to help discover visual patterns that would otherwise go unnoticed to the human eye [8, 9]. Much work in this area has focused on assessing the role of PET and CT image features as potential biomarkers in NSCLC [5, 15]. Among them, tumor uniformity has received particular attention, for it is believed that more heterogeneous tumors are also more aggressive and correlate with poorer outcomes [8, 10, 12, 16].

Still, few studies [17–19] have investigated the correlations between CT and PET features on a quantitative basis. Understanding such relationships, however, is important not only to eliminate potentially redundant features from radiomics models but also to uncover relationships that can provide insight into NSCLC itself. The identification of histological types [20, 21] is also essential to therapy planning due to the differences that exist in the overall outcome for the different subtypes [22, 23].

The objective of this study is to investigate the correlations between PET texture features, CT texture features, and histological subtypes in non-small-cell lung cancer evaluated with [^{18}F]FDG PET/CT.

Materials and Methods

Patients

We retrospectively evaluated the baseline PET/CT scans (before any treatment) of 81 patients with suspicious lung cancer. All scans were performed and evaluated by the University Unit of Nuclear Medicine, Perugia Hospital (Perugia, Italy), between November 2005 and January 2011. The inclusion criteria were as follows: (a) the presence of a single, clearly identifiable lung lesion (both at CT and PET) with overall volume >3 cm^3 in both imaging modalities and (b) a histologically confirmed diagnosis of NSCLC. The characteristics of the patient series are summarized in Table 1.

PET/CT Image Acquisition

All patients gave written informed consent to undergo PET/CT for clinical purposes and to accept that their data could be used in anonymous form for scientific studies. After a 12-h fast the serum glucose levels of the subjects were assessed to make sure that this was lower than 120 mg/dL (6.66 mmol/L). Subsequently, the weight and height of all the subjects were measured. [^{18}F] FDG was administered intravenously to each subject (340–450 MBq) followed by saline solution (250–500 ml). Sixty minutes after the radiopharmaceutical injection the patients were invited to lie down comfortably in supine position within the gantry

Table 1. Characteristics of the patient series

Characteristic	Value
Age (years)	67.4 (range 45.5–84.4)
Gender	
Male	67 (82.7 %)
Female	14 (17.2 %)
Overall stage	
IA	22 (27.2 %)
IB	21 (25.9 %)
IIA	7 (8.6 %)
IIB	6 (7.4 %)
IIIA	23 (28.5 %)
IIIB	1 (1.2 %)
IV	1 (1.2 %)
Clinical T stage[a]	
T1	28 (34.6 %)
T2	36 (44.4 %)
T3	11 (13.6 %)
T4	6 (7.4 %)
Clinical N stage[a]	
N0	53 (65.4 %)
N1	12 (14.8 %)
N2	16 (19.8 %)
Clinical M stage[a]	
M0	80 (98.8 %)
M1	1 (1.2 %)
Histology	
Adenocarcinoma	35 (43.2 %)
Squamous cell carcinoma	31 (38.3 %)
Large cell carcinoma	8 (9.9 %)
Mixed/unspecified	7 (8.6 %)

[a]TMN version 7.0

and recommended to maintain their arms raised to decrease beam-hardening artifacts.

Conventional low-dose CT images for attenuation correction were acquired in helical mode with X-ray peak voltage between 120 and 140 Kv and tube current between 80 and 302 mA—the latter being automatically adjusted to maintain a constant noise level (GE Healthcare "Smart mA" system). Each slice was reconstructed in a matrix of dimension of 512 px × 512 px, corresponding to a thickness of 3.75 mm and in-plane pixel spacing of ≈ 0.98 mm × 0.98 mm. PET scanning was performed with a two-dimensional technique in the caudo-cranial direction from the proximal one third of the femur to the skull. The dimension of the in-plane matrix was 128 px × 128 px (corresponding to ≈ 4.6 mm × 4.6 mm) and the slice thickness 3.2 mm. The images were reconstructed on the axial, coronal, and sagittal plane views and were corrected for attenuation *via* a standard iterative algorithm (ordered subset expectation maximization). The total PET scan time ranged between 24 and 28 min.

Table 2. Image features and related symbols

Description	Modality	
	CT	PET
Volume	CT_{vol}	MTV
Maximum value	CT_{max}	SUV_{max}
Average value	CT_{mean}	SUV_{mean}
Standard deviation	CT_{std}	SUV_{std}
Skewness	CT_{skw}	SUV_{skw}
Kurtosis	CT_{krt}	SUV_{krt}
Entropy	CT_{ent}	SUV_{ent}
Uniformity	CT_{uni}	SUV_{uni}

Lesion Delineation and Feature Extraction

Segmentation of the volume of interest (VOI) was carried out on the open-access LIFEx platform v4.0 [24] (IMIV/CEA, Orsay, France). The delineation of the lesions was performed manually, slice-by-slice, and separately for the PET and CT scans (no automatic transposition of the VOIs from PET to CT or *vice versa* was involved). The CT segmentation was limited to those parts of the lesions that appeared as solid. Only primary lesions were considered in the study: suspicious lymph nodes and/or secondary malignant growths were not included. The process was accomplished by one radiation oncologist (I.P., > 10-year experience) and one nuclear medicine specialist (B.P., > 15-year experience). Sample cases with the manually delineated lesions are shown in Fig. 1.

Feature extraction was based on custom routines developed on the Matlab platform (MathWorks, Natick, USA). We considered the following features (Table 2): volume, max, mean, standard deviation, skewness [25, p. 620], kurtosis [25, p. 620], entropy [26], and uniformity [8]. We applied windowing to all the features except volume, which represents the raw volume of the manually segmented regions of interest without any further pre-processing. For the CT features we used a window of 300 HU centered at 125 HU (same settings as in [27]); for PET features a window of 50 SUV centered at 25 SUV. Histogram-based features (*i.e.*, entropy and homogeneity) for both PET and CT were computed by discretizing the windows into 256 levels. No other pre-processing procedures such as image filtering and/or smoothing were applied.

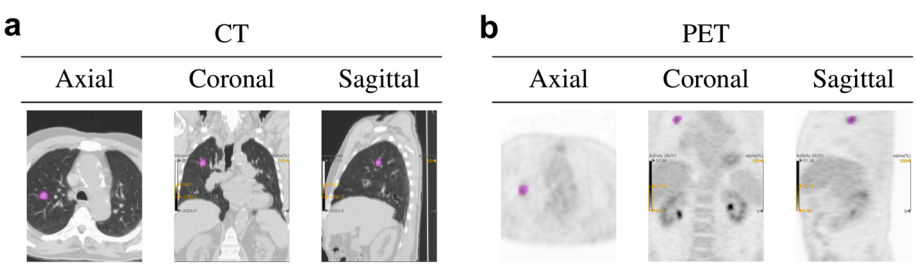

Fig. 1 **a** CT and **b** PET scans of one sample case showing the manually delineated lesions.

Table 3. Levels of correlation strength

Value of ρ	Interpretation
$-1.0 \le \rho < -0.9$	Very strong negative correlation
$-0.9 \le \rho < -0.7$	Strong negative correlation
$-0.7 \le \rho < -0.4$	Moderate negative correlation
$-0.4 \le \rho < -0.1$	Weak negative correlation
$-0.1 \le \rho < 0.0$	Negligible negative correlation
$0.0 \le \rho < 0.1$	Negligible positive correlation
$0.1 \le \rho < 0.4$	Weak positive correlation
$0.4 \le \rho < 0.7$	Moderate positive correlation
$0.7 \le \rho < 0.9$	Strong positive correlation
$0.9 \le \rho \le 1.0$	Very strong positive correlation

Statistical Analysis

Intra- (CT-CT, PET-PET) and inter-modality (CT-PET) correlations among the image features were investigated using non-parametric Spearman's rank correlation coefficient (ρ). The use of Spearman's ρ is a safe choice for a number of reasons, specifically: it does not rely on the assumption of normally distributed variables, is appropriate when one or both variables are skewed, and is robust to outliers [28]. The p value was estimated *via* Student's t approximation with $(n-2)$ degrees of freedom, being n the number of samples [29]. A correlation value was considered significant if $p \le \alpha/c_1$, where α is the significance level ($\alpha = 0.05$ in this case) and c_1 is the Bonferroni's correction coefficient for multiple tests. Since we carried out $f \times (f-1)$ intra-modality pairwise comparisons of features and f^2 inter-modality comparisons, the correction coefficient was the following:

$$c_1 = 2 \times f^2 - f \tag{1}$$

where f is the number of features considered in the study ($f = 8$). The statistically significant values were finally stratified into ten levels of correlation strength as shown in Table 3.

Correlations between feature values and histological subtypes were evaluated *via* non-parametric Wilcoxon rank sum test [25, p. 604] and in a one-*vs.*-other manner—*i.e.*, the feature values of each subtype were compared against those of all the other subtypes. Groups with less than eight cases were excluded; therefore, we carried out the following pairwise evaluations: (1) adenocarcinoma *vs.* others, (2) large-cell carcinoma *vs.* others, and (3) squamous cell carcinoma *vs.* others. Correlation was considered significant if $p \le \alpha/c_2$, where c_2 is again the Bonferroni correction coefficient for multiple tests. In this case, since we evaluated $f = 8$ CT features and as many PET features for each of the three above pairs, we had the following:

$$c_2 = 3 \times 2 \times f = 6f \tag{2}$$

Table 4. Intra-modality correlation between CT features

	CT_{max}	CT_{mean}	CT_{ent}	CT_{std}	CT_{skw}	CT_{krt}	CT_{uni}
CT_{vol}	$\rho = 0.756$ ($p < 0.001$)	$\rho = 0.599$ ($p < 0.001$)	$\rho = 0.156$ ($p = 0.164$)	$\rho = -0.179$ ($p = 0.109$)	$\rho = 0.124$ ($p = 0.271$	$\rho = 0.659$ ($p < 0.001$)	$\rho = 0.046$ ($p = 0.680$)
CT_{max}		$\rho = 0.581$ ($p < 0.001$)	$\rho = 0.422$ ($p < 0.001$)	$\rho = 0.248$ ($p < 0.025$)	$\rho = 0.544$ ($p < 0.001$)	$\rho = 0.887$ ($p < 0.001$)	$\rho = -0.221$ ($p = 0.048$)
CT_{mean}			$\rho = 0.184$ ($p = 0.100$)	$\rho = -0.025$ ($p = 0.827$)	$\rho = -0.168$ ($p = 0.135$)	$\rho = 0.492$ ($p < 0.001$)	$\rho = 0.046$ ($p = 0.685$)
CT_{ent}				$\rho = 0.830$ ($p < 0.001$)	$P = 0.385$ ($p < 0.001$)	$\rho = 0.194$ ($p = 0.083$)	$\rho = -0.939$ ($p < 0.001$)
CT_{std}					$\rho = 0.496$ ($p < 0.001$)	$\rho = 0.035$ ($p = 0.754$)	$\rho = -0.860$ ($p < 0.001$)
CT_{skw}						$\rho = 0.487$ ($p < 0.001$)	$\rho = -0.351$ ($p < 0.001$)
CT_{krt}							$\rho = 0.014$ ($p = 0.901$)

Table 5. Intra-modality correlation between PET features

	SUV_{max}	SUV_{mean}	PET_{ent}	PET_{std}	PET_{skw}	PET_{krt}	PET_{uni}
MTV	$\rho = 0.630$ ($p < 0.001$)	$\rho = 0.526$ ($p < 0.001$)	$\rho = 0.707$ ($p < 0.001$)	$\rho = 0.526$ ($p < 0.001$)	$\rho = 0.068$ ($p = 0.548$)	$\rho = -0.013$ ($p = 0.911$)	$\rho = -0.685$ ($p < 0.001$)
SUV_{max}		$\rho = 0.895$ ($p < 0.001$)	$\rho = 0.928$ ($p < 0.001$)	$\rho = 0.962$ ($p < 0.001$)	$\rho = 0.285$ ($p = 0.010$)	$\rho = 0.079$ ($p = 0.482$)	$\rho = -0.908$ ($p < 0.001$)
SUV_{mean}			$\rho = 0.928$ ($p < 0.001$)	$\rho = 0.909$ ($p < 0.001$)	$\rho = -0.051$ ($p = 0.653$)	$\rho = -0.231$ ($p = 0.038$)	$\rho = -0.938$ ($p < 0.001$)
PET_{ent}				$\rho = 0.937$ ($p < 0.001$)	$\rho = 0.063$ ($p = 0.574$)	$\rho = -0.159$ ($p = 0.155$)	$\rho = -0.995$ ($p < 0.001$)
PET_{std}					$\rho = 0.217$ ($p = 0.052$)	$\rho = -0.041$ ($p = 0.714$)	$\rho = -0.922$ ($p < 0.001$)
PET_{skw}						$\rho = 0.896$ ($p < 0.001$)	$\rho = -0.007$ ($p = 0.947$)
PET_{krt}							$\rho = 0.207$ ($p = 0.064$)

Table 6. Inter-modality correlations between PET and CT features

	CT_{vol}	CT_{max}	CT_{mean}	CT_{ent}	CT_{std}	CT_{skw}	CT_{krt}	CT_{uni}
MTV	$\rho = 0.818$ ($p < 0.001$)	$\rho = 0.678$ ($p < 0.001$)	$\rho = 0.575$ ($p < 0.001$)	$\rho = 0.093$ ($p = 0.411$)	$\rho = -0.163$ ($p = 0.146$)	$\rho = 0.140$ ($p = 0.212$)	$\rho = 0.645$ ($p < 0.001$)	$\rho = 0.080$ ($p = 0.480$)
SUV_{max}	$\rho = 0.603$ ($p < 0.001$)	$\rho = 0.395$ ($p = 0.001$)	$\rho = 0.522$ ($p < 0.001$)	$\rho = -0.023$ ($p = 0.840$)	$\rho = -0.263$ ($p = 0.018$)	$\rho = -0.137$ ($p = 0.222$)	$\rho = 0.410$ ($p < 0.001$)	$\rho = 0.193$ ($p = 0.084$)
SUV_{mean}	$\rho = 0.586$ ($p < 0.001$)	$\rho = 0.403$ ($p = 0.001$)	$\rho = 0.566$ ($p < 0.001$)	$\rho = 0.042$ ($p = 0.712$)	$\rho = -0.190$ ($p = 0.089$)	$\rho = -0.169$ ($p = 0.131$)	$\rho = 0.379$ ($p = 0.001$)	$\rho = 0.138$ ($p = 0.220$)
PET_{ent}	$\rho = 0.650$ ($p < 0.001$)	$\rho = 0.425$ ($p < 0.001$)	$\rho = 0.611$ ($p < 0.001$)	$\rho = -0.055$ ($p = 0.627$)	$\rho = -0.299$ ($p = 0.007$)	$\rho = -0.194$ ($p = 0.082$)	$\rho = 0.448$ ($p < 0.001$)	$\rho = 0.238$ ($p = 0.033$)
PET_{std}	$\rho = 0.479$ ($p < 0.001$)	$\rho = 0.250$ ($p = 0.024$)	$\rho = 0.492$ (p < 0.001)	$\rho = -0.095$ ($p = 0.396$)	$\rho = -0.297$ ($p = 0.007$)	$\rho = -0.257$ ($p = 0.021$)	$\rho = 0.293$ ($p = 0.008$)	$\rho = 0.240$ ($p = 0.031$)
PET_{skw}	$\rho = -0.073$ ($p = 0.516$)	$\rho = -0.027$ ($p = 0.811$)	$\rho = -0.044$ ($p = 0.693$)	$\rho = -0.050$ ($p = 0.654$)	$\rho = -0.044$ ($p = 0.699$)	$\rho = 0.021$ ($p = 0.854$)	$\rho = 0.029$ ($p = 0.799$)	$\rho = 0.039$ ($p = 0.727$)
PET_{krt}	$\rho = -0.071$ ($p = 0.526$)	$\rho = -0.002$ ($p = 0.988$)	$\rho = -0.131$ ($p = 0.243$)	$\rho = 0.063$ ($p = 0.574$)	$\rho = 0.071$ ($p = 0.528$)	$\rho = 0.125$ ($p = 0.266$)	$\rho = -0.006$ ($p = 0.954$)	$\rho = -0.093$ ($p = 0.407$)
PET_{uni}	$\rho = -0.643$ ($p < 0.001$)	$\rho = -0.419$ ($p < 0.001$)	$\rho = -0.606$ ($p < 0.001$)	$\rho = 0.058$ ($p = 0.606$)	$\rho = 0.297$ ($p = 0.007$)	$\rho = 0.197$ ($p = 0.078$)	$\rho = -0.445$ ($p < 0.001$)	$\rho = -0.241$ ($p = 0.030$)

Table 7. Correlations between PET/CT features and histological types (box plots available in Figs. 2 and 3)

Feature	Histotype (a)	Histotype (b)	Median (a)	Median (b)	*p* value
CT_{vol}	Squamous cell	Others	78.535	20.206	< 0.001
MTV	Squamous cell	Others	29.171	10.957	< 0.001
SUV_{mean}	Squamous cell	Others	5.168	3.577	< 0.001
PET_{ent}	Squamous cell	Others	3.807	3.191	< 0.001
PET_{std}	Squamous cell	Others	2.984	1.722	< 0.001
PET_{uni}	Squamous cell	Others	0.028	0.047	< 0.001
SUV_{max}	Adenocarcinoma	Others	8.036	14.102	< 0.001
SUV_{mean}	Adenocarcinoma	Others	3.424	4.774	< 0.001
PET_{ent}	Adenocarcinoma	Others	3.178	3.646	< 0.001
PET_{std}	Adenocarcinoma	Others	1.567	2.613	< 0.001
PET_{uni}	Adenocarcinoma	Others	0.050	0.033	< 0.001

Results

Intra-modality analysis of CT features (Table 4) identified three pairs of features with strong positive correlation, eight with moderate positive correlation, one with strong negative correlation, and another one with very strong negative correlation. For PET features (Table 5), the same analysis revealed very strong positive correlation for five pairs of features, strong positive correlation for three pairs, moderate positive correlation for three, moderate negative correlation for one, and very strong negative correlation for four. Inter-

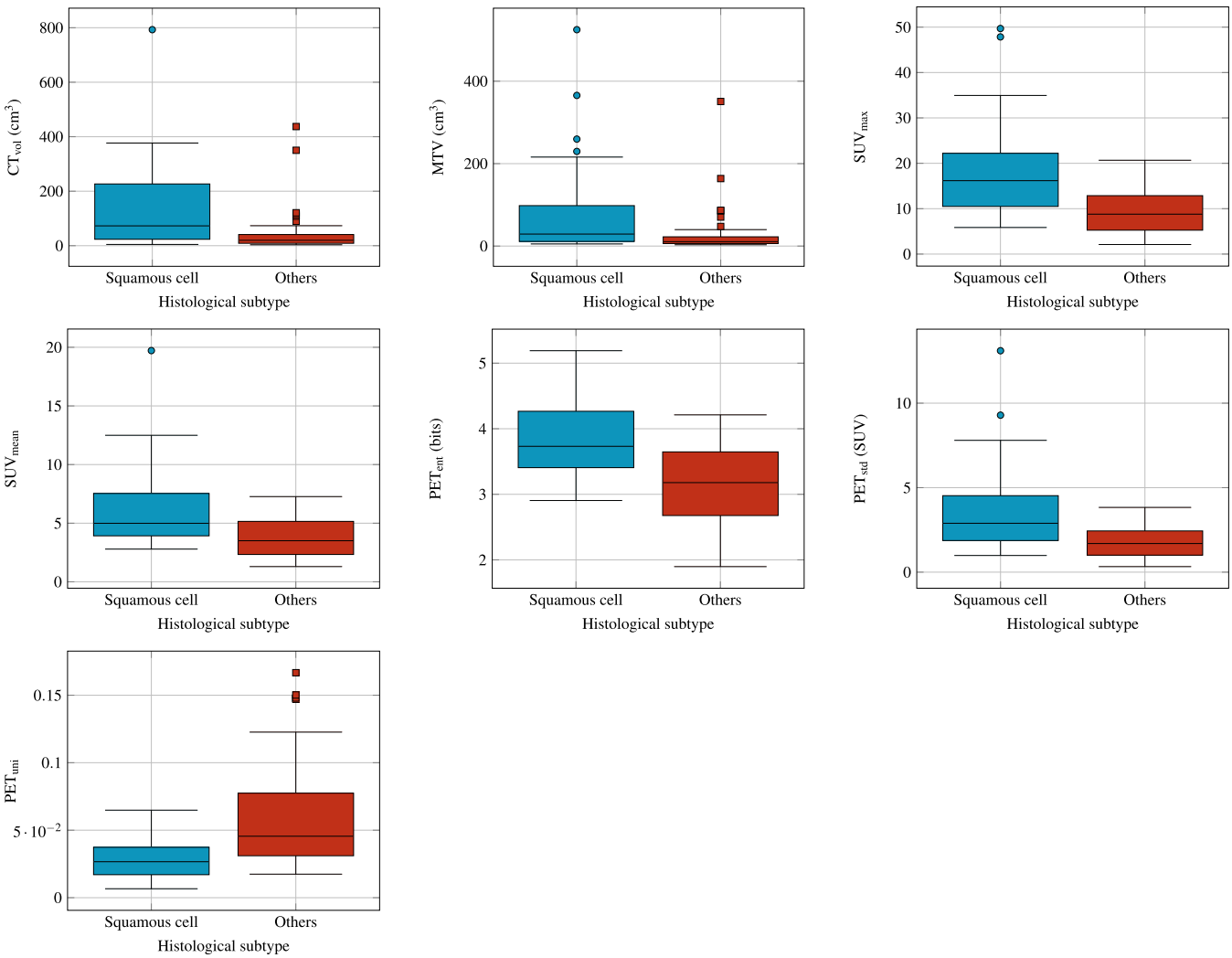

Fig. 2 Correlations between PET/CT features and histological types. Box plots of the features with significant difference between squamous cell carcinoma and the other histological types (Table 5).

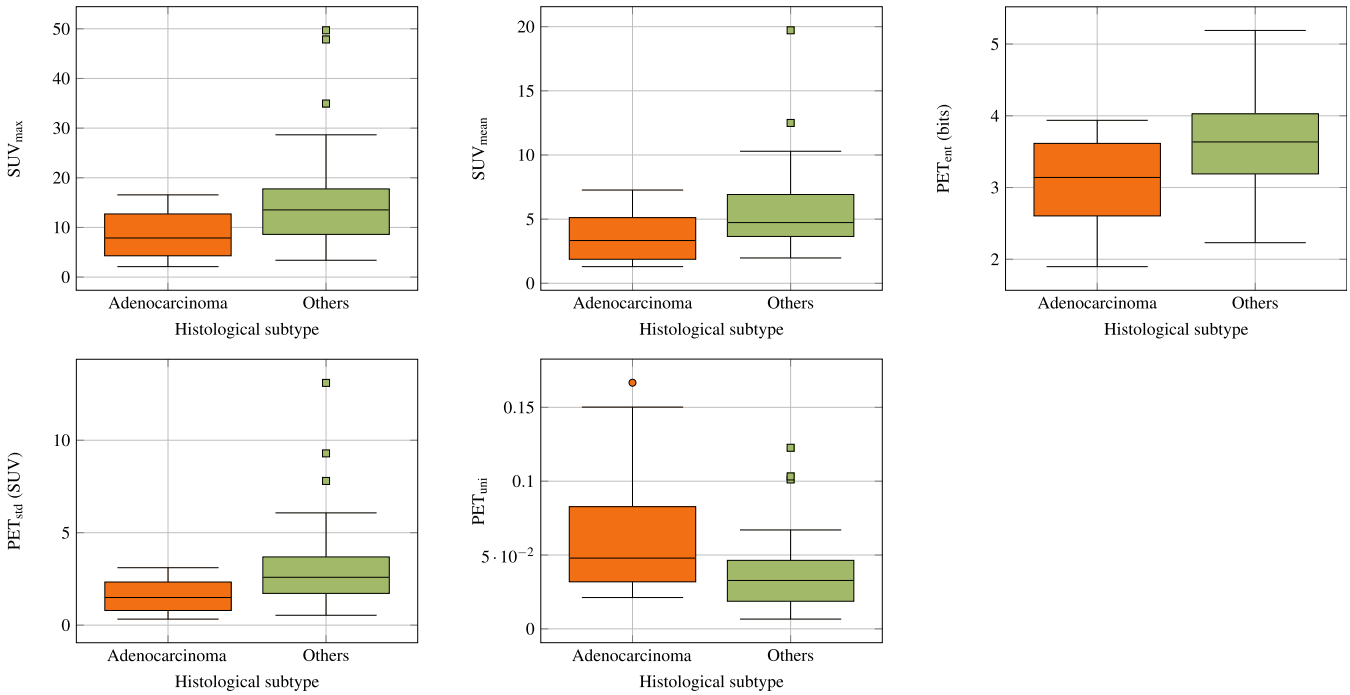

Fig. 3 Correlations between PET/CT features and histological types. Box plots of the features with significant difference between adenocarcinoma and the other histological types (Table 5).

modality correlation analysis between PET and CT features (Table 6) returned one pair of features with strong positive correlation, 15 pairs with moderate positive correlation, one with weak positive correlation, and four with moderate negative correlation.

Regarding the histological type (Table 7 and Figs. 2 and 3), squamous cell carcinomas had significantly larger volumes (CT_{vol}, MTV) than the other subtypes. Evaluated at PET, squamous cell carcinomas also exhibited higher uptake (SUV_{max}, SUV_{mean}), stronger variability (SUV_{std}, SUV_{ent}), and lower uniformity (SUV_{uni}) than the other subtypes. By contrast, adenocarcinomas exhibited significantly lower uptake (SUV_{max}, SUV_{mean}), weaker variability (SUV_{std}, SUV_{ent}), and higher uniformity (SUV_{uni}) than the other subtypes.

Discussion

Although biopsy is a necessary exam to perform the histological classification of the disease, radiomics might have an increasing clinical role, as it provides a non-invasive *in vivo* method able to characterize lesions, thus obtaining a sort of an "*in vivo* biopsy." This finding could be of pivotal importance—particularly when the clinical conditions of the subject and/or the lesion's site make traditional biopsy unfeasible. Other interesting information offered by radiomics include prognostic data and response to treatment. Although the literature shows an increasing trend in publishing papers on the impact of radiomics in radiology and nuclear medicine [7, 11, 15], further studies are required to better standardize the methodology and strengthen the results. Non-small-cell lung cancer has been investigated by using radiomics in various papers [9, 12, 30, 31], for an *in vivo* biomarker of disease could be strategic to promptly adequately treat patients. Our study contributes to the *in vivo* characterization of disease as it evaluates correlations between [^{18}F] FDG PET features, CT features, and histological types.

Some of the correlation results presented in the "Results" section are easily explained in terms of the feature definitions themselves. For intra-modality pairs of features (*i.e.*, CT-CT and PET-PET), a positive correlation between mean and maximum values is something one would reasonably expect. Likewise, consider that both entropy and standard deviation indicate the amount of disorder and variability, and are therefore awaited to correlate positively with each other. Also, the two are presumed to correlate negatively with uniformity, which, by contrast, is a measure of orderliness. This suggests that using more than one parameter among entropy, standard deviation and uniformity (or others of the same this kind) may be redundant and unnecessary. Of the three, the standard deviation is arguably the most convenient, for it can be computed directly on the image data without requiring histogram binning.

Intra-modality correlation analysis between CT features indicated a link between the volume of the lesion (CT_{vol}) and the tissue density: there was a strong positive correlation with the maximum density (CT_{max}) and a moderate positive one with the average density (CT_{mean}). To the best of our

knowledge this is a novel finding not previously reported in the related literature. Its potential implications are promising, though their role in the clinical management is still unclear at the moment and should be further investigated in future studies.

Intra-modality correlation analysis between PET features showed a strong positive correlation between the metabolic activity of the lesion (SUV_{max} and SUV_{mean}) and its variability (SUV_{std}, SUV_{ent}). Conversely—but equivalently—the correlation was strongly negative between the radiotracer uptake (SUV_{max}, SUV_{mean}) and its degree of uniformity (SUV_{uni}) This suggests that the role of PET heterogeneity parameters as independent biomarkers in NSCLC [31] might need to be evaluated further.

Inter-modality correlation analysis among PET and CT features revealed a moderate positive correlation between the tissue density (CT_{mean}) and the radiotracer uptake (SUV_{max}, SUV_{mean}), a result which agrees with the findings of Giesel et al. [19], albeit their study involved lymph nodes and not primary lesions. The dimension of the lesions (CT_{vol}, MTV) also showed a moderate positive correlation with the uptake values (SUV_{max}, SUV_{mean}), which is consisted with the results reported by Brunese et al. [17]. However, the measures of heterogeneity at CT (CT_{std}, CT_{ent}, and CT_{uni}) were not significantly correlated with the metabolic activity evaluated at PET.

With respect to the relationships between radiomics features and histological types, we found that squamous cell carcinomas had significantly larger volumes (CT_{vol}, MTV) and FDG uptake (SUV_{max}, SUV_{mean}) than the other histological types. Notably, the uptake finding is in good agreement with the results recently obtained by de Geus-Oei et al. [32]. The adenocarcinomas, by contrast, had lower uptake than the other subtypes, which is consistent with the results of Brunese et al. [17], although the difference did not reach statistical significance in their study. The disorder-related parameters computed from PET (SUV_{ent}, SUV_{std}, and SUV_{uni}) data showed a significantly higher degree of heterogeneity in squamous cell carcinoma than in the other histological types, whereas the reverse occurred with adenocarcinomas, which had lower heterogeneity than the other types.

In previous works higher rates of radiotracer uptake in patients with NSCLC correlated positively to proliferation rate [33], tumor doubling time [34], and, generally, worse outcome [9]. Likewise, the degree of heterogeneity at PET has been associated with higher risk of local recurrence, disease-specific survival, and, in general, worse prognosis [31].

However, in our cohort of patients squamous-cell carcinomas were significantly more advanced cases than the other histological types (median stage IIB *vs.* IB), whereas there was no statistically significant difference between the adenocarcinomas and the other histological types (median stage IB). These data are in agreement with the natural history of the disease with squamous cell carcinomas achieving larger tumor volumes in the lung primary lesion before giving nodal and distant metastases. It is therefore not surprising that in our cohort squamous cell carcinomas were significantly more advanced than non-squamous subtypes (median stage IIB *vs.* IB). This stratification also reflects the one reported by Fukui et al. [23] on a much larger cohort of patients ($n = 2059$).

To summarize, the clinical implications of this investigation are represented by the possibility to differentiate squamous-cell carcinomas *vs.* adenocarcinomas by means of radiomics features. If confirmed in future studies, this could have important implications in the early diagnostic process of NSCLC allowing to plan a prompt therapeutic strategy without biopsy.

Furthermore, the correlation between lesion volume and tissue density, if confirmed in other studies, may be clinically relevant as it shows that larger lesions are also denser, which is likely to be related to higher proliferation rate and malignancy. Our results, in particular, showed a positive (albeit moderate) correlation between radiopharmaceutical uptake, volume, and density of the lesions—*i.e.*, larger and denser lesions had also higher metabolic activity, which is generally associated with tumor proliferation and poor prognosis.

Conclusions

The application of texture analysis and artificial intelligence techniques to PET and CT data offers new opportunities for the management of patients with oncologic disorders. Texture analysis has the potential to capture information beyond what is visible to the human eye in an objective and repeatable way. Besides, compared with biopsies, texture analysis is non-invasive and provides information over the whole tumor. In this context the evaluation of NSCLC *via* quantitative imaging techniques (radiomics) is a topic where the scientific interest is currently high [7, 9, 11, 15, 31]. It is in fact believed that the extraction of *in vivo* biomarkers from PET/CT data can play an important role in patient assessment and treatment. In this scenario the present study has uncovered interesting correlations between CT features, PET features, and histological subtypes in patients with NSCLC which have only marginally been investigated so far. Our results may improve diagnosis and patient stratification, and could lead to better understanding of NSCLC. In particular, our study contributes to the *in vivo* characterization of disease as it evaluates correlations between PET features, CT features, and histological types.

This work is not exempt from limitations: among them the retrospective nature of the study and the relatively small sample size. Larger cohorts of patients and prospective studies will be needed to confirm these preliminary findings and translate the results into the clinical practice. The present investigation was also eminently cross-sectional—*i.e.*, no attempt was made at determining the potential of the image features at predicting major outcomes such as overall and disease-specific survival. Likewise, proliferation indexes and/or receptor expression could not be investigated due to the lack of specific metadata. Future work should also focus on defining standardized methodology for image acquisition and extraction.

Funding Information. This work was partially supported by the Department of Engineering at the Università degli Studi di Perugia, Italy, under the Fundamental Research Scheme 2018 (M.L. Fravolini and F. Bianconi); by the Italian Ministry of Education, University and Research (MIUR) within the Individual Annual Funding for Fundamental Research "FFABR" 2018 (F. Bianconi and I. Palumbo); and by the Fondazione Cassa di Risparmio di Perugia (Perugia, Italy) with the project Application of Artificial Intelligence methods to PET/CT for computer-assisted diagnosis (grant no. 2015.0389 013).

Compliance with Ethical Standards

Ethical Approval

All the procedures performed in this study were in accordance with the ethical standards of the institutional and/or national research committee and with the 1964 Helsinki declaration and its later amendments or comparable ethical standards. Formal ethical approval was not required due to the retrospective nature of the study and the analysis of anonymous clinical data.

Informed Consent

All patients gave written informed consent to undergo PET/CT for clinical purposes and to accept that their data could be used in anonymous form for scientific studies.

Conflict of Interest

The authors declare that they have no conflict of interest.

References

1. American Cancer Society. Cancer statistics center, 2018. Available online at: https://cancerstatisticscenter.cancer.org/#!/. Last accessed on Jul. 9, 2018
2. Molina JR, Yang CPSD et al (2008) Non-small cell lung cancer: epidemiology, risk factors, treatment, and survivorship. Mayo Clinic Proc 83:584–594
3. Palumbo B, Buresta Nuvoli TS et al (2014) SPECT and PET serve as molecular imaging techniques and in vivo biomarkers for brain metastases. Int J Mol Sci 15:9878–9893
4. Chao F, Zhang H (2012) PET/CT in the staging of the non-small-cell lung cancer. J biomed Biotechnol. Art. 783739
5. Scrivener M, de Jong EEC, van Timmeren T et al (2016) Radiomics applied to lung cancer: a review. Transl Cancer Res 5:398–409
6. Dennie C, Thornhill R, Sethi-Virmani V et al (2016) Role of quantitative computed tomography texture analysis in the differentiation of primary lung cancer and granulomatous nodules. Quant Imaging Med Surg 6:6–15
7. Kirienko M, Cozzi L, Rossi A, Voulaz E, Antunovic L, Fogliata A, Chiti A, Sollini M (2018) Ability of FDG PET and CT radiomics features to differentiate between primary and metastatic lung lesions. Eur J Nucl Med Mol Imaging 45:1649–1660
8. Ganeshan B, Panayiotou E, Burnand K, Dizdarevic S, Miles K (2012) Tumour heterogeneity in non-small cell lung carcinoma assessed by CT texture analysis: a potential marker of survival. Eur Radiol 22:796–802
9. Nappi A, Gallicchio R, Simeon V, Nardelli A, Pelagalli A, Zupa A, Vita G, Venetucci A, di Cosola M, Barbato F, Storto G (2015) FDG-PET/CT parameters as predictors of outcome in inoperable NSCLC patients. Radiol Oncol 49:320–326
10. Sacconi B, Anzidei M, Leonardi A, Boni F, Saba L, Scipione R, Anile M, Rengo M, Longo F, Bezzi M, Venuta F, Napoli A, Laghi A, Catalano C (2017) Analysis of CT features and quantitative texture analysis in patients with lung adenocarcinoma: a correlation with EGFR mutations and survival rates. Clin Radiol 72:443–450
11. Bianconi F, Fravolini ML, Bello-Cerezo R et al (2018) Evaluation of shape and textural features from CT as prognostic biomarkers in non-small cell lung cancer. Anticancer Res 38:2155–2160
12. Ravanelli M, Farina D, Morassi N et al (2013) Texture analysis of advanced non-small cell lung cancer (NSCLC) on contrast-enhanced computed tomography: prediction of the response to the first-line chemotherapy. Eur Radiol 23:3450–3455
13. Sun R, Limkin EJ, Vakalopoulou M, Dercle L, Champiat S, Han SR, Verlingue L, Brandao D, Lancia A, Ammari S, Hollebecque A, Scoazec JY, Marabelle A, Massard C, Soria JC, Robert C, Paragios N, Deutsch E, Ferté C (2018) A radiomics approach to assess tumour-infiltrating CD8 cells and response to anti-PD-1 or anti-PD-L1 immunotherapy: an imaging biomarker, retrospective multicohort study. Lancet Oncol 19:1180–1191
14. Cook CJR, Azad G, Owczarczyk K et al (2018) Challenges and promises of PET radiomics. Int J Radiat Oncol Biol Phys 102:1083–1089
15. Sollini M, Cozzi L, Antunovic L, Chiti A, Kirienko M (2017) PET radiomics in NSCLC: state of the art and a proposal for harmonization of methodology. Sci Rep 7 Art no 7:358
16. Bashir U, Siddique MM, McLean E et al (2016) Imaging heterogeneity in lung cancer: techniques, applications, and challenges. Am J Roentgenol 207:534–543
17. Brunese L, Greco B, Setola FR, Lassandro F, Guarracino MR, de Rimini M, Piccolo S, de Rosa N, Muto R, Bianco A, Muto P, Grassi R, Rotondo A (2013) Non-small cell lung cancer evaluated with quantitative contrast-enhanced CT and PET-CT: net enhancement and standardized uptake values are related to tumour size and histology. Med Sci Monit 19:95–101
18. Wu W, Parmar C, Grossmann P et al (2016) Exploratory study to identify radiomics classifiers for lung cancer histology. Front Oncol 6 Art no:71
19. Giesel FL, Schneider F, Kratochwil C, Rath D, Moltz J, Holland-Letz T, Kauczor HU, Schwartz LH, Haberkorn U, Flechsig P (2017) Correlation between SUVmax and CT radiomic analysis using lymph node density in PET/CT-based lymph node staging. J Nucl Med 58:282–287
20. Saad M, Choi T-S (2018) Computer-assisted subtyping and prognosis for non-small cell lung cancer patients with unresectable tumor. Comput Med Imaging Graph 67:1–8
21. Zhu X, Dong D, Chen Z, Fang M, Zhang L, Song J, Yu D, Zang Y, Liu Z, Shi J, Tian J (2018) Radiomic signature as a diagnostic factor for histologic subtype classification of non-small cell lung cancer. Eur Radiol 28:2772–2778
22. Kawase A, Yoshida J, Ishii G, Nakao M, Aokage K, Hishida T, Nishimura M, Nagai K (2012) Differences between squamous cell carcinoma and adenocarcinoma of the lung: are adenocarcinoma and squamous cell carcinoma prognostically equal? Jpn J Clin Oncol 42:189–195
23. Fukui T, Taniguchi T, Kawaguchi K, Fukumoto K, Nakamura S, Sakao Y, Yokoi K (2015) Comparisons of the clinicopathological features and survival outcomes between lung cancer patients with adenocarcinoma and squamous cell carcinoma. Gen Thorac Cardiovasc Surg 63:507–513
24. Nioche C, Orlhac F, Boughdad S, Reuzé S, Goya-Outi J, Robert C, Pellot-Barakat C, Soussan M, Frouin F, Buvat I (2018) LIFEx: a freeware for radiomic feature calculation in multimodality imaging to accelerate advances in the characterization of tumor heterogeneity. Cancer Res 78:4786–4789
25. du Prel J-B, Röhrig B, Hommel G, Blettner M (2010) choosing statistical tests. Dtsch Arztebl Int 2010 107: 343–348
26. Aerts HJWL, Velazquez ER, Leijenaar RTH, et al. (2014) Decoding tumour phenotype by noninvasive imaging using a quantitative radiomics approach. Nat Commun 5 art. No. 4006
27. Oikonomou A, Khalvati F, Tyrrell PN, Haider MA, Tarique U, Jimenez-Juan L, Tjong MC, Poon I, Eilaghi A, Ehrlich L, Cheung P (2018) Radiomics analysis at PET/CT contributes to prognosis of recurrence and survival in lung cancer treated with stereotactic body radiotherapy. Sci Rep 8:4003
28. Schober F, Boer C, Schwarte LA (2018) Correlation coefficients: appropriate use and interpretation. Anesth Analg 126:1763–1768
29. Zar JH (1972) Testing of the spearman rank correlation coefficient. J Am Stat Assoc 67:578–580
30. Zhang J, Gold KA, Lin HY, Swisher SG, Xing Y, Lee JJ, Kim ES, William WN Jr (2015) Relationship between tumor size and survival in non-small-cell lung cancer (NSCLC): an analysis of the surveillance, epidemiology, and end results (SEER) registry. J Thorac Oncol 10:682–690

31. Pyka T, Bundschuh RA, Andratschke N, Mayer B, Specht HM, Papp L, Zsótér N, Essler M (2015) Textural features in pre-treatment [F18]-FDG-PET/CT are correlated with risk of local recurrence and disease-specific survival in early stage NSCLC patients receiving primary stereotactic radiation therapy. Radiat Oncol 10:100
32. de Geus-Oei L-F, van Krieken JHJM, Aliredjo RP et al (2007) Biological correlates of FDG uptake in non-small cell lung cancer. Lung Cancer 55:79–87
33. Vesselle H, Schmidt RA, Pugsley JM et al (2000) Lung cancer proliferation correlates with [F-18] fluorodeoxyglucose uptake by positron emission tomography. Clin Cancer Res 6:3837–3844
34. Duhaylongsod FG, Lowe VJ, Patz EF Jr, Patz EF Jr, Vaughn AL, Coleman RE, Wolfe WG (1995) Lung tumor growth correlates with glucose metabolism measured by fluoride-18 fluorodeoxyglucose positron emission tomography. Ann Thorac Surg 60:1348–1352